Bosonic pair production and squeezing for optical phase measurements in long-lived dipoles coupled to a cavity

Bhuvanesh Sundar,^{1,2} Diego Barberena,^{1,2} Asier Piñeiro Orioli,^{1,2} Anjun Chu,^{1,2} James K. Thompson,² Ana Maria Rey,^{1,2} and Robert J. Lewis-Swan^{3,4}

¹ Center for Theory of Quantum Matter, University of Colorado, Boulder, CO 80309, USA

² JILA, NIST, Department of Physics, University of Colorado, Boulder, CO 80309, USA

³ Homer L. Dodge Department of Physics and Astronomy,

The University of Oklahoma, Norman, OK 73019, USA

⁴ Center for Quantum Research and Technology, The University of Oklahoma, Norman, OK 73019, USA

We propose to simulate bosonic pair creation using large arrays of long-lived dipoles with multilevel internal structure coupled to an undriven optical cavity. Entanglement between the atoms, generated by the exchange of virtual photons through a common cavity mode, grows exponentially fast and is described by two-mode squeezing (TMS) of effective bosonic quadratures. The mapping between an effective bosonic model and the natural spin description of the dipoles allows us to realize the analog of optical homodyne measurements via straightforward global rotations and population measurements of the electronic states, and we propose to exploit this for quantum-enhanced sensing of an optical phase (common and differential between two ensembles). We discuss a specific implementation based on Sr atoms and show that our sensing protocol is robust to sources of decoherence intrinsic to cavity platforms. Our proposal can open unique opportunities for the observation of continuous variable entanglement in atomic systems and associated applications in next-generation optical atomic clocks.

The production of entangled pairs of quantum particles is a process with relevance across broad areas of quantum science, ranging from fundamental investigations of quantum mechanics [1–3] and exotic phenomena in high energy physics and QED [4–6], to technological applications in quantum communication [7], amplification of quantum signals [8], metrology [9–11], and information processing [12].

Pairs of entangled photons are a workhorse of quantum optics, typically generated via processes such as, e.g., four-wave mixing (FWM) of optical fields in a nonlinear medium [13]. Complementary efforts have also sought to realize pair production of entangled bosonic atoms using the intrinsic nonlinearity provided by contact interactions in ultracold gases [6, 14-19]. A common example are spinor Bose-Einstein condensates (BECs) [20– 26, wherein spin-changing collisions between atoms of different internal spin states simulate a pair production process that is analogous to degenerate FWM of optical fields [27]. While atomic realizations present distinct advantages and opportunities relative to optical systems, including entanglement of massive particles and longer interaction times where the dynamics can be highly nonperturbative, spatial dynamics of the atomic clouds can sometimes add unwanted complexity to the pair creation process. For example, in spinor BECs it is typically assumed that spatial motion is frozen out so that the internal spin dynamics can be amenably described by a simple single-mode model [28, 29].

In this Letter, we outline a proposal to simulate a pair production process through light-mediated interactions between atoms confined in an optical cavity and exploit it for quantum-enhanced metrology. Pairs of entangled excitations are generated by the exchange of virtual photons between a quartet of internal spin states coupled to a common, far-detuned cavity mode, in a process analogous to FWM. The pinning of the atoms in a deep optical lattice supported by the cavity, in combination with the global range of the effective interaction [30], avoids undesirable motional decoherence and can enable the study of large systems without treating complex multi-mode dynamics such as those encountered in, e.g., spinor BECs [29]. The exploitation of light-mediated exchange interactions realized by coupling an optical transition to an undriven cavity complements prior work involving Raman transitions [31, 32], and avoids potential sources of technical noise introduced by driving the cavity with an external field, such as fluctuations in the drive intensity or detuning. Nevertheless, our proposal can in principle be extended to these systems.

In optical systems, the generation of entangled photons is well known to lead to excess quantum fluctuations in the phase and amplitude quadratures of each photon mode, but suppressed relative fluctuations of the combined quadratures of the two modes. This form of inter-mode entanglement, described by two-mode squeezing (TMS), can be diagnosed using homodyne techniques, whereby optical quadratures are measured by mixing the squeezed light with a strong classical reference field [33]. Atomic homodyne techniques have also been developed and realized in spinor BECs, whereby the condensate takes the role of the phase reference, but these require careful mixing of multiple internal states [20, 34], or alternatively nonlinear readout protocols to exploit the correlated noise [35]. Here, we demonstrate that by engineering TMS using long-lived optical transitions coupled

by a common cavity mode, the quadrature squeezing can be accessed and exploited for quantum-enhanced sensing via a standard Ramsey sequence employing rotations and population measurements on the optical transitions. The four-level realization of the TMS lets us design protocols to sense rotations about any collective quadrature, including differential phases and sum phases imprinted on the atoms. We verify that our protocol is robust to typical sources of decoherence in cavity-QED realizations and thus can be immediately relevant for state-of-theart time and frequency standards, while simultaneously opening new opportunities for the observation and probing of continuous variable entangled states.

Engineered FWM - We consider an ensemble of atoms trapped by a deep one-dimensional magic optical lattice within an optical cavity, such that the spatial dynamics are effectively frozen. A single cavity mode, with angular frequency ω_c and power decay linewidth κ , couples to a long-lived optical transition, with angular frequency ω_a and natural decay rate $\gamma \ll \kappa$, between a manifold of ground (g) and excited (e) states with single-photon Rabi frequency $2g_0$ [see Fig. 1(a)]. We focus on the fardetuned limit, $|\Delta| = |\omega_c - \omega_a| \gg g_0 \sqrt{N}$, κ , for N atoms, where the dynamics is almost unitary. The cavity field can be adiabatically eliminated and serves only to mediate effective interactions between the atoms [36]. For concreteness of the following discussion, here we consider a system based on the Zeeman levels of the ${}^{1}S_{0}$ (g) and ${}^{3}P_{0}$ (e) electronic states in ${}^{87}Sr$ with F = 9/2, which are separated by an optical transition frequency forming the basis of state-of-the-art optical lattice clocks [37]. However, our discussion can be generalized to alternative implementations using, e.g., two spatially divided ensembles to emulate the multiple internal transitions [32, 38].

We assume the atomic ensemble is prepared with an equal population of atoms in the electronic states $|g, m = -9/2\rangle$ and $|e, m = 9/2\rangle$ where m labels the spin projection of the Zeeman sublevel along the quantization axis set to be perpendicular to the cavity axis (e.g. by an external magnetic field). In Ref. [39] (see also Fig. 1) we verify that under this initial condition, the description of the cavity-mediated dynamics can be restricted to a quartet of states, $|g, m = \pm 9/2\rangle$ and $|e, m = \pm 9/2\rangle$, as the population of other Zeeman sublevels is suppressed by a combination of collective effects and favourable Clebsch-Gordan coefficients [39, 40]. The atomic evolution is then described by the effective spin Hamiltonian [36, 39],

$$\hat{H} = \hbar \chi \left(\hat{S}_A^+ + \hat{S}_B^+ \right) \left(\hat{S}_A^- + \hat{S}_B^- \right) + \hbar \delta \left(\hat{S}_B^z - \hat{S}_A^z \right). \tag{1}$$

Hereafter, we denote the m=-9/2(9/2) manifold as the A(B) ensemble. We have introduced collective operators $\hat{S}_A^+ = \sum_{i=1}^N |e,A\rangle_i \, \langle g,A|_i, \, \hat{S}_B^+ = -\sum_i |e,B\rangle_i \, \langle g,B|_i$ and $\hat{S}_\alpha^z = 1/2 \sum_i \left(|e,\alpha\rangle_i \, \langle e,\alpha|_i - |g,\alpha\rangle_i \, \langle g,\alpha|_i\right)$ for $\alpha=A,B$, where the summation runs over all N atoms. The non-traditional sign convention for the B ensem-

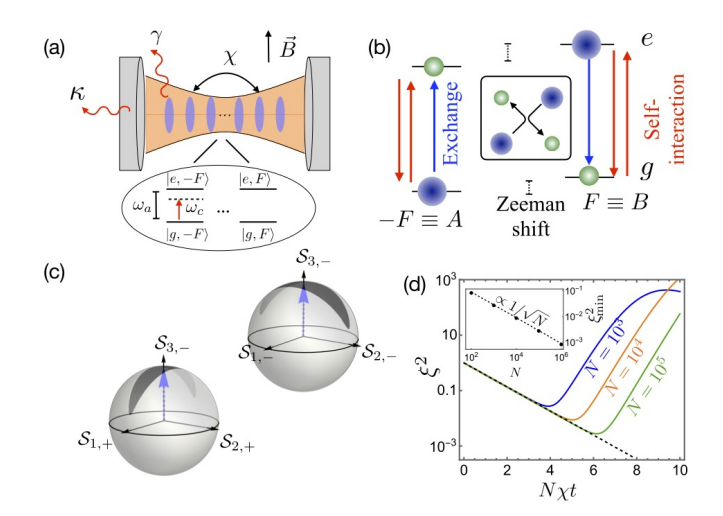


FIG. 1. (a) Schematic of cavity implementation: Interactions (χ) between multilevel atoms (internal structure shown in inset) are mediated by exchange of virtual photons through a common cavity mode of angular frequency $\omega_c = \omega_a + \Delta$ where Δ is the detuning and ω_a is the atomic transition angular frequency. The cavity leaks photons through the mirrors at rate κ and the atoms undergo spontaneous emission at rate γ . A magnetic field perpendicular to the cavity axis provides a Zeeman shift, and sets the quantization direction. (b) Possible exchange processes (blue) and self-interactions (red) caused by cavity-mediated interactions. (c) Visualization of the spin squeezing generated during the dynamics, in the combined basis of the A and B manifolds. Blue arrows label the Bloch vector. (d) Squeezing, quantified by the normalized variance $\xi^2 = N(\Delta S_{1,-})^2 = N(\Delta S_{2,+})^2$, for $\delta = N\chi/2$ and different atom numbers N. The UPA prediction (dashed line) agrees with TWA calculations (solid lines) until corrections beyond UPA become important (see text). The minimum squeezing is $\xi_{\min}^2 \approx 0.88/\sqrt{N}$ as shown in the inset.

ble accounts for the differing sign of Clebsch-Gordan coefficients for the relevant transitions in each ensemble, which we absorb in the raising/lowering operators rather than Hamiltonian definition for convenience. The cavity detuning Δ controls the strength of the interaction, $\chi \approx -g_F^2/\Delta$ where the adjusted Rabi frequency $2g_F = 2g_0\sqrt{F/(F+1)}$ includes an additional factor $\sqrt{F/(F+1)}$ arising from Clebsch-Gordan coefficients [39]. A relative Zeeman shift, $\propto \delta$, splits the energies of the two ensembles.

The first term of Eq. (1) is a flip-flop process that includes: i) an exchange of an excitation between the A and B ensembles, e.g., $\hat{S}_A^+\hat{S}_B^- + h.c.$, and ii) a self-interaction $\hat{S}_A^+\hat{S}_A^- + \hat{S}_B^+\hat{S}_B^-$. Both can be understood as the simultaneous destruction of a pair of particles in two atomic levels and subsequent creation of a pair in two levels, which is analogous to the process of FWM familiar from quantum and atom optics. We rigorize this analogy by defining Schwinger boson operators $\hat{a}_{g,\alpha}$ and $\hat{a}_{e,\alpha}$ via

 $\hat{S}^+_{\alpha}=\hat{a}^\dagger_{e,\alpha}\hat{a}_{q,\alpha}$ to rewrite the spin Hamiltonian as,

$$\begin{split} \hat{H}_{\text{FWM}} &= \hbar \chi \left(\hat{a}_{e,A}^{\dagger} \hat{a}_{g,A} + \hat{a}_{e,B}^{\dagger} \hat{a}_{g,B} \right) \left(\hat{a}_{g,A}^{\dagger} \hat{a}_{e,A} + \hat{a}_{g,B}^{\dagger} \hat{a}_{e,B} \right) \\ &+ \frac{\hbar \delta}{2} \left(\hat{a}_{g,A}^{\dagger} \hat{a}_{g,A} + \hat{a}_{e,B}^{\dagger} \hat{a}_{e,B} - \hat{a}_{e,A}^{\dagger} \hat{a}_{e,A} - \hat{a}_{g,B}^{\dagger} \hat{a}_{g,B} \right), \end{split}$$

where the first line describes a set of FWM processes between the four Zeeman sublevels. The Hamiltonian (2) is closely related to that realized via spin-changing interactions in spin-1 BECs [39] under the assumption that all atoms are restricted to a single common spatial mode. This assumption is fundamentally absent in cavity-QED implementations [30, 32, 36] as the infinite-range interactions are physically generated by the atomic coupling to a single common cavity mode, which can be made uniform by selective loading of the atoms in the spatial lattice or by adopting a ring cavity configuration.

Dynamics of pair creation – In quantum optics it is common to make an undepleted pump approximation (UPA) [41] to study FWM dynamics, corresponding to replacing $\hat{a}_{g,A}, \hat{a}_{e,B} \sim \sqrt{N/2}$ in $\hat{H}_{\rm FWM}$. For simplicity, we have assumed that the two pump modes are equally populated and treat the general case with unequal pump populations in Ref. [39]. Further assuming $\delta = N\chi/2$ to effectively remove the mean-field interaction shift due to the self-interaction terms $\chi(\hat{S}_A^+\hat{S}_A^- + \hat{S}_B^+\hat{S}_B^-)$ [39] we obtain,

$$\hat{H}_{\rm TMS} = \frac{N\hbar\chi}{2} \left(\hat{a}_{e,A}^{\dagger} \hat{a}_{g,B}^{\dagger} + \text{h.c.} \right). \tag{3}$$

This final form elucidates a resonant production of pairs of bosons, or equivalently the correlated transfer of pairs of atoms to the internal levels $|e,A\rangle$ and $|g,B\rangle$. Using $\hat{H}_{\rm TMS}$, the number of entangled particles is $\bar{n}(t) = \langle \hat{a}_{e,A}^{\dagger} \hat{a}_{e,A} + \hat{a}_{g,B}^{\dagger} \hat{a}_{g,B} \rangle = 2 \sinh^2(N\chi t/2)$ [25, 42]. We verify this prediction in [39].

Two-mode squeezing for enhanced metrology with an optical transition - It is well established in quantum optics that the Hamiltonian Eq. (3) generates squeezing of combined two-mode quadrature fluctuations [43]. Considering $\chi > 0$ without loss of generality, within the UPA \dot{H} produces squeezing along two bosonic quadratures labelled Y_{+} and X_{-} and anti-squeezing along conjugate quadratures X_{+} and Y_{-} [39], with exponentially fast suppression or growth of the associated quantum noise $\langle (\Delta \hat{X}_{\pm})^2 \rangle = \frac{1}{2} e^{\pm N\chi t}$ and $\langle (\Delta \hat{Y}_{\pm})^2 \rangle = \frac{1}{2} e^{\mp N\chi t}$. Importantly for our proposal, the two-mode quadrature squeezing can be observed in collective spin operators that act on our four-level system, up to corrections beyond UPA [39] that we will argue are irrelevant in practice. Specifically, the squeezed quadratures can be directly mapped to a combination of spin operators, $\sqrt{\frac{N}{2}}\hat{X}_{-} = \hat{S}_{1,-} \equiv$ $\hat{S}_B^x - \hat{S}_A^y$ and $\sqrt{\frac{N}{2}}\hat{Y}_+ = \hat{S}_{2,+} \equiv \hat{S}_B^y + \hat{S}_A^x$. Correspondingly,

the anti-squeezed quadratures are $\sqrt{\frac{N}{2}}\hat{Y}_{-}=\hat{S}_{2,-}\equiv \hat{S}_{B}^{y}-\hat{S}_{A}^{x}$ and $\sqrt{\frac{N}{2}}\hat{X}_{+}=\hat{S}_{1,+}\equiv \hat{S}_{B}^{x}+\hat{S}_{A}^{y}$.

We can visualize the squeezed quantum noise of the combined spin state corresponding to the A and B transitions on a pair of coupled Bloch spheres defined by axes $(S_{1,-}, S_{2,-}, S_{3,-})$ and $(S_{1,+}, S_{2,+}, S_{3,-})$ that share a common vertical component $S_{3,-} = S_B^z - S_A^z$ and for which the corresponding operators obey standard SU(2) commutation relations [39]. As shown in Fig. 1(c), the state is squeezed in both Bloch spheres, $(\Delta \hat{S}_{1,-})^2 = (\Delta \hat{S}_{2,+})^2 = Ne^{-N\chi t}/4$, relative to the level of the initial state which is separable.

The UPA prediction for the squeezing, $(\Delta S_{1,-})^2$ and $(\Delta S_{2,+})^2$, is verified in Fig. 1(d) by comparing to a calculation of the variances based on a numerical simulation of the full multilevel cavity implementation, and we find excellent agreement up to $\bar{n} \sim 0.76\sqrt{N}$. The multilevel cavity dynamics are obtained using a truncated Wigner approximation (TWA), which approximates the quantum dynamics by averaging over an ensemble of mean field trajectories with initial conditions chosen to reproduce the quantum fluctuations of the initial state [44–48]. We include all possible exchange processes between the complete set of 4F+2 ground and excited atomic levels in our TWA simulation, including, e.g., those mediated by photons with polarization perpendicular to the quantization axis [39, 49].

A Ramsey protocol that uses only collective rotations and population measurements of the collective spins encoded in the A and B manifolds can be used to take advantage of the squeezing in the Bloch sphere for enhanced sensing of phase shifts imprinted on the optical transition. The protocol is analogous to optical homodyne techniques in quantum optics, as well as atomic homodyne [34, 50] or measurements of squeezing in spin-1 BECs [51, 52]. However, as our atomic realization is based on four internal levels, as opposed to three in spin-1 BECs, we do not require any coherent mixing of the $F = \pm 9/2$ manifolds. This also distinguishes our approach from prior demonstrations of interferometry with Dicke-like states realized in spin-1 BECs [21], which treat the $m_F = \pm 1$ modes as the two internal levels of a collective spin-1/2 system and uses a Holland-Burnett-type protocol [53]. Such an approach is sensitive to decoherence [54] and readout errors [55], while in our system it would also add the complex requirement of engineering a coupling between the $F = \pm 9/2$ states.

Here, we present Ramsey protocols for measuring sum and difference optical phases imprinted on the atoms, illustrated in Fig. 2. Measuring differential phases has several applications including gravimetry [56], measuring gravitational redshifts [57–60], and detecting gravitational waves [61, 62] and dark matter [63]. Measuring the sum phase is useful for improving state-of-the-art optical atomic clocks.

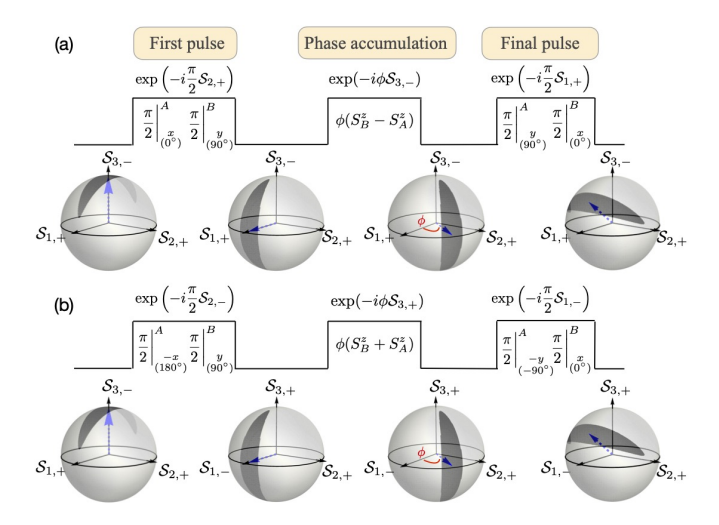


FIG. 2. (a) Ramsey sequence to measure a differential clock phase shift imprinted on the atoms. A first $\pi/2$ pulse rotates the Bloch vector to the equator. Next, a phase accumulation rotates the Bloch vector about $S_B^z - S_A^z$ by an angle ϕ , before a final $\pi/2$ pulse rotates the Bloch vector for readout via measuring $\hat{S}_B^z - \hat{S}_A^z$. (b) Ramsey sequence to measure the sum phase imprinted on the atoms. The first $\pi/2$ pulse defines the squeezed distribution on a joint Bloch sphere of A and B defined by the axes $(S_{1,-}, S_{2,+}, S_{3,+})$. After phase accumulation about $\hat{S}_B^z + \hat{S}_A^z$, the final pulse again rotates the Bloch vector for readout via measuring $\hat{S}_B^z + \hat{S}_A^z$. In both cases, dashed blue arrows mark the Bloch vector at each stage. The subscript x(y) for the pulses denote the axis of rotation $S_x(S_y)$, and the degree $0^{\circ}(90^{\circ})$ in the subscript conveys the same information via the phase of the laser pulse.

To measure a differential phase imprinted by a rotation about $S_B^z - S_A^z$, we begin our protocol with a $\pi/2$ -pulse that rotates atoms in the A ensemble about S^x and those in the B ensemble by S^y , i.e implements $\exp(-i\frac{\pi}{2}\hat{S}_{2,+})$. Next, we accumulate a relative phase shift by a rotation of ϕ about $-S_A^z$ and S_B^z (i.e. $S_{3,-}$), and finally apply a second $\pi/2$ -pulse which rotates atoms in the A and B ensembles about S^y and S^x , i.e. implements $\exp(-i\frac{\pi}{2}\hat{S}_{1,+})$. The action of this pulse sequence on the state is best visualized by looking at the spin distribution in the lower Bloch sphere in Fig. 1(c), as shown in Fig. 2(a). The final pulse converts the rotation \hat{U}_ϕ into a measurable change in the difference in atomic inversions

$$\langle \hat{S}_B^z - \hat{S}_A^z \rangle = \frac{N}{2} \sin \phi. \tag{4}$$

This Ramsey sequence does not imprint any information about the differential phase on the upper Bloch sphere in Fig. 1(c), as we discuss in Ref. [39].

The sum phase, imprinted by a collective rotation around $S_{3,+} \equiv S_A^z + S_B^z$, can be similarly inferred by another Ramsey protocol shown in Fig. 2(b). Note that neither Bloch sphere in Fig. 1(c) has $S_{3,+}$ as an axis. Therefore, the first pulse in this Ramsey protocol, implementing $\exp(-i\frac{\pi}{2}\hat{S}_{2,-})$, is chosen such that it rotates

the axes in the Bloch sphere from $(S_{1,+}, S_{2,+}, S_{3,-})$ to $(-S_{3,+}, S_{2,+}, S_{1,-})$, thus introducing $S_{3,+}$ into relevance. The remainder of the sequence proceeds analogously to that for the differential phase.

The sensitivity of both our protocols is given by

$$(\Delta\phi)^2 \equiv \frac{(\Delta O)^2}{(d\langle\hat{O}\rangle/d\phi)^2} = \frac{e^{-N\chi t}}{N} + \frac{\bar{n}(\bar{n}+2)}{4N^2} \tan^2\phi, (5)$$

where \hat{O} is the observable measured. Eq. (5) is valid within the UPA and predicts an advantage relative to the SQL $(\Delta\phi)^2=1/N$ for any non-zero \bar{n} . Moreover, we predict sub-SQL sensitivity for a wide dynamic range of ϕ lying in the region $|\tan\phi|<2\sqrt{N}/\bar{n}$, which can be $\mathcal{O}(1)$. In Fig. 1(d) we compare the result in Eq. (5) with that obtained by a TWA calculation accounting for pump depletion, and find excellent agreement up to $\bar{n}\sim 0.76\sqrt{N}$.

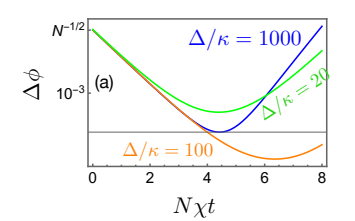
The sensitivity [Eq. (5)] can have additional terms due to unequal pump populations, corrections beyond the UPA model (see below), and decoherence (further below), all of which degrade the sensitivity. We focus on the latter effects here and discuss population fluctuations in Ref. [39], where we find they lead to at worst comparable degradation. The leading corrections beyond the UPA model of \hat{H}_{TMS} can be captured by iteratively modifying the UPA to include depletion of the pump states $|g,A\rangle$ and $|e,B\rangle$ by $\bar{n}/2$. This is achieved by setting $\hat{a}_{g,A},\hat{a}_{e,B}\approx\sqrt{\frac{N-\bar{n}}{2}}$ where $\bar{n}=2\sinh^2\frac{N\chi t}{2}$ is taken to be the original UPA result as a first approximation. Making this correction has two physical consequences [39]: i) the effective nonlinearity $\chi(N-\bar{n})/2$ driving pair production is reduced relative to the UPA, and ii) the pair production is no longer resonant as the Zeeman shift $\delta = \chi N/2$ is static and does not completely cancel the mean-field shift introduced by the self-interaction terms in Eq. (2). For $1 \ll \bar{n} \ll N$ we then obtain the beyond-UPA sensitivity [39]

$$(\Delta\phi)^2 \approx \frac{1}{2N\bar{n}} + \frac{\bar{n}^3}{2N^3} + \frac{\bar{n}(\bar{n}+2)}{4N^2} \tan^2\phi.$$
 (6)

The optimal sensitivity remains enhanced relative to the standard quantum limit (SQL), with a lower bound of $(\Delta\phi)^2 = 2/(3^{3/4}N^{3/2})$ that occurs for $\bar{n} = \sqrt{N}/3^{1/4}$, in agreement with the TWA results in Fig. 1(d).

Decoherence – Dissipative noise in our system intrinsically arises from superradiant decay, at a rate $\Gamma \approx g_F^2 \kappa/\Delta^2$, due to leakage of the photons that mediate the effective atom-atom interaction from the cavity, and single particle spontaneous emission into free space at the rate γ . While both are deleterious for sensing, we show that our protocol can achieve sub-SQL sensitivity even with these sources of decoherence.

The effects of collective decay can be treated by solving a Lindblad master equation with jump operator $\hat{L} = \sqrt{\Gamma}(\hat{S}_A^- + \hat{S}_B^-)$, which captures the dominant



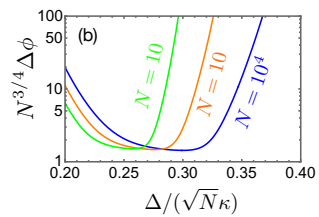


FIG. 3. (a) Sensitivity versus time for different cavity detunings Δ , and C=10 and $N=10^5$. The best sensitivity is achieved at an optimum time for each Δ . (b) Scaled best sensitivity, $N^{3/4}\Delta\phi$, versus Δ . In each case, the minima occur at similar $\Delta/(\sqrt{N}\kappa)$, and have similar values (up to logarithmic corrections).

process where an emitted photon polarized along the quantization axis is lost from the cavity [39]. Spontaneous emission is included through jump operators $\hat{L}_i = \sqrt{\gamma}(\hat{\sigma}_{A,i}^- + \hat{\sigma}_{B,i}^-)$, where $\hat{\sigma}_{m,i}^-$ is the spin-lowering operator in the manifold with azimuthal quantum number m for the i^{th} atom.

In Fig. 3(a) we plot the sensitivity as a function of time in the presence of decoherence for a range of cavity detunings. We observe that for every detuning there is an optimum time when the best sensitivity is achieved. This optimum time balances the gain obtained by reaching a higher \bar{n} versus the loss in squeezing due to decoherence. By optimising this interplay via Δ (thus tuning χ relative to Γ and γ) we obtain a best achievable sensitivity [39]

$$(\Delta\phi)^2 = \frac{\sqrt{2\ln(2NC)}}{N^{3/2}\sqrt{C}},\tag{7}$$

for $\Delta = \frac{\kappa\sqrt{NC}}{2\sqrt{\ln(2NC)}}$, with $C = 4g_F^2/\kappa\gamma$ the single-atom cooperativity. This sensitivity is only slightly reduced relative to the ideal case [see Fig. 1(d) and Eq. (6)] and is competitive with the best sensitivities achievable with the paradigmatic approach of one-axis twisting when decoherence is properly accounted for [64–66].

Outlook – Our proposal offers new opportunities to study and exploit the exponentially rapid generation of entanglement in atomic systems, driven by connections to well established concepts in quantum optics. Moreover, our proposal highlights new possibilities for the realization and investigation of diverse models of bosonic pair production in highly tunable quantum simulators featuring spin-spin interactions.

Acknowledgments – We thank M. Affolter, A. Carter, and T. Bilitewski for a careful reading and comments on the manuscript. This work is supported by the AFOSR grants FA9550-18-1-0319 and FA9550-19-1-0275, by the DARPA and ARO grant W911NF-16-1-0576, by the NSF JILA-PFC PHY-1734006, QLCI-OMA -2016244, by the U.S. Department of Energy, Office of Science, National Quantum Information Science Research Centers Quantum Systems Accelerator, and by NIST.

- N. Brunner, D. Cavalcanti, S. Pironio, V. Scarani, and S. Wehner, Rev. Mod. Phys. 86, 419 (2014).
- [2] M. D. Reid, P. D. Drummond, W. P. Bowen, E. G. Cavalcanti, P. K. Lam, H. A. Bachor, U. L. Andersen, and G. Leuchs, Rev. Mod. Phys. 81, 1727 (2009).
- [3] R. Lopes, A. Imanaliev, A. Aspect, M. Cheneau, D. Boiron, and C. I. Westbrook, Nature **520**, 66 (2015).
- [4] P. Hauke, D. Marcos, M. Dalmonte, and P. Zoller, Phys. Rev. X 3, 041018 (2013).
- [5] V. Kasper, F. Hebenstreit, M. Oberthaler, and J. Berges, Physics Letters B 760, 742 (2016).
- [6] J. Hu, L. Feng, Z. Zhang, and C. Chin, Nature Physics 15, 785 (2019).
- [7] J. Yin, Y. Cao, Y.-H. Li, S.-K. Liao, L. Zhang, J.-G. Ren, W.-Q. Cai, W.-Y. Liu, B. Li, H. Dai, G.-B. Li, Q.-M. Lu, Y.-H. Gong, Y. Xu, S.-L. Li, F.-Z. Li, Y.-Y. Yin, Z.-Q. Jiang, M. Li, J.-J. Jia, G. Ren, D. He, Y.-L. Zhou, X.-X. Zhang, N. Wang, X. Chang, Z.-C. Zhu, N.-L. Liu, Y.-A. Chen, C.-Y. Lu, R. Shu, C.-Z. Peng, J.-Y. Wang, and J.-W. Pan, Science 356, 1140 (2017), https://www.science.org/doi/pdf/10.1126/science.aan3211
- [8] A. Roy and M. Devoret, Comptes Rendus Physique 17, 740 (2016), quantum microwaves / Micro-ondes quantiques.
- [9] J.-W. Pan, Z.-B. Chen, C.-Y. Lu, H. Weinfurter, A. Zeilinger, and M. Żukowski, Rev. Mod. Phys. 84, 777 (2012).
- [10] P.-A. Moreau, E. Toninelli, T. Gregory, and M. J. Padgett, Nature Reviews Physics 1, 367 (2019).
- [11] L. Pezzè, A. Smerzi, M. K. Oberthaler, R. Schmied, and P. Treutlein, Rev. Mod. Phys. 90, 035005 (2018).
- [12] P. Kok, W. J. Munro, K. Nemoto, T. C. Ralph, J. P. Dowling, and G. J. Milburn, Rev. Mod. Phys. 79, 135 (2007).
- [13] G. S. Agarwal, Quantum optics (Cambridge University Press, 2012).
- [14] R. Bücker, J. Grond, S. Manz, T. Berrada, T. Betz, C. Koller, U. Hohenester, T. Schumm, A. Perrin, and J. Schmiedmayer, Nat. Phys. 7, 608 (2011).
- [15] M. Bonneau, J. Ruaudel, R. Lopes, J.-C. Jaskula, A. Aspect, D. Boiron, and C. I. Westbrook, Phys. Rev. A 87, 061603(R) (2013).
- [16] Y.-Q. Zou, L.-N. Wu, Q. Liu, X.-Y. Luo, S.-F. Guo, J.-H. Cao, M. K. Tey, and L. You, Proceedings of the National Academy of Sciences 115, 6381 (2018), https://www.pnas.org/content/115/25/6381.full.pdf.
- [17] S. S. Hodgman, R. I. Khakimov, R. J. Lewis-Swan, A. G. Truscott, and K. V. Kheruntsyan, Phys. Rev. Lett. 118, 240402 (2017).
- [18] J.-C. Jaskula, M. Bonneau, G. B. Partridge, V. Krach-malnicoff, P. Deuar, K. V. Kheruntsyan, A. Aspect, D. Boiron, and C. I. Westbrook, Phys. Rev. Lett. 105, 190402 (2010).
- [19] F. Borselli, M. Maiwöger, T. Zhang, P. Haslinger, V. Mukherjee, A. Negretti, S. Montangero, T. Calarco, I. Mazets, M. Bonneau, and J. Schmiedmayer, Phys. Rev. Lett. 126, 083603 (2021).
- [20] C. Gross, H. Strobel, E. Nicklas, T. Zibold, N. Bar-Gill, G. Kurizki, and M. K. Oberthaler, Nature 480, 219 (2011).
- [21] B. Lücke, M. Scherer, J. Kruse, L. Pezzé, F. Deuret-

- zbacher, P. Hyllus, J. Peise, W. Ertmer, J. Arlt, L. Santos, A. Smerzi, and C. Klempt, Science **334**, 773 (2011).
- [22] E. M. Bookjans, C. D. Hamley, and M. S. Chapman, Phys. Rev. Lett. 107, 210406 (2011).
- [23] A. T. Black, E. Gomez, L. D. Turner, S. Jung, and P. D. Lett, Phys. Rev. Lett. 99, 070403 (2007).
- [24] L. Zhao, J. Jiang, T. Tang, M. Webb, and Y. Liu, Phys. Rev. A 89, 023608 (2014).
- [25] A. Qu, B. Evrard, J. Dalibard, and F. Gerbier, Phys. Rev. Lett. 125, 033401 (2020).
- [26] K. Kim, J. Hur, S. J. Huh, S. Choi, and J.-y. Choi, Phys. Rev. Lett. 127, 043401 (2021).
- [27] E. S. Polzik and J. Ye, Phys. Rev. A 93, 021404(R) (2016).
- [28] C. K. Law, H. Pu, and N. P. Bigelow, Phys. Rev. Lett. 81, 5257 (1998).
- [29] J. Jie, Q. Guan, S. Zhong, A. Schwettmann, and D. Blume, Phys. Rev. A 102, 023324 (2020).
- [30] M. A. Norcia, R. J. Lewis-Swan, J. R. K. Cline, B. Zhu, A. M. Rey, and J. K. Thompson, Science 361, 259 (2018).
- [31] S. J. Masson, M. D. Barrett, and S. Parkins, Phys. Rev. Lett. 119, 213601 (2017).
- [32] E. J. Davis, G. Bentsen, L. Homeier, T. Li, and M. H. Schleier-Smith, Phys. Rev. Lett. 122, 010405 (2019).
- [33] C. Gardiner and P. Zoller, Quantum noise: a handbook of Markovian and non-Markovian quantum stochastic methods with applications to quantum optics (Springer Science & Business Media (New York), 2004).
- [34] J. Peise, I. Kruse, K. Lange, B. Lücke, L. Pezzè, J. Arlt, W. Ertmer, K. Hammerer, L. Santos, A. Smerzi, and C. Klempt, Nat. Commun. 6, 1 (2015).
- [35] D. Linnemann, H. Strobel, W. Muessel, J. Schulz, R. J. Lewis-Swan, K. V. Kheruntsyan, and M. K. Oberthaler, Phys. Rev. Letters 117, 013001 (2016).
- [36] J. A. Muniz, D. Barberena, R. J. Lewis-Swan, D. J. Young, J. R. K. Cline, A. M. Rey, and J. K. Thompson, Nature 580, 602 (2020).
- [37] A. D. Ludlow, M. M. Boyd, J. Ye, E. Peik, and P. O. Schmidt, Rev. Mod. Phys. 87, 637 (2015).
- [38] A. Periwal, E. S. Cooper, P. Kunkel, J. F. Wienand, E. J. Davis, and M. Schleier-Smith, Nature 600, 630 (2021).
- [39] "See Supplemental Material at [URL will be inserted by publisher].".
- [40] M. A. Norcia, M. N. Winchester, J. R. Cline, and J. K. Thompson, Sci. Adv. 2, e1601231 (2016).
- [41] C. Gerry and P. Knight, "Nonclassical light," in *Introductory Quantum Optics* (Cambridge University Press (Cambridge), 2004) p. 150–194.
- [42] A. I. Lvovsky, Photonics: Scientific Foundations, Technology and Applications 1, 121 (2015).
- [43] D. F. Walls and G. J. Milburn, *Quantum Optics*, 2nd ed. (Springer, 2008).
- [44] B. Zhu, A. M. Rey, and J. Schachenmayer, New Journal of Physics 21, 082001 (2019).

- [45] S. Lepoutre, J. Schachenmayer, L. Gabardos, B. Zhu, B. Naylor, E. Maréchal, O. Gorceix, A. M. Rey, L. Vernac, and B. Laburthe-Tolra, Nature Communications 10, 1714 (2019).
- [46] J. Schachenmayer, A. Pikovski, and A. M. Rey, Phys. Rev. X 5, 011022 (2015).
- [47] A. Patscheider, B. Zhu, L. Chomaz, D. Petter, S. Baier, A.-M. Rey, F. Ferlaino, and M. J. Mark, Phys. Rev. Research 2, 023050 (2020).
- [48] B. Sundar, K. C. Wang, and K. R. A. Hazzard, Physical Review A 99, 043627 (2019).
- [49] A. Piñeiro Orioli, J. K. Thompson, and A. M. Rey, arXiv e-prints , arXiv:2106.00019 (2021), arXiv:2106.00019 [quant-ph].
- [50] W. Muessel, H. Strobel, D. Linnemann, D. B. Hume, and M. K. Oberthaler, Phys. Rev. Lett. 113, 103004 (2014).
- [51] C. D. Hamley, C. S. Gerving, T. M. Hoang, E. M. Bookjans, and M. S. Chapman, Nat. Phys. 8, 305 (2012).
- [52] F. Anders, L. Pezzè, A. Smerzi, and C. Klempt, Phys. Rev. A 97, 043813 (2018).
- [53] M. J. Holland and K. Burnett, Phys. Rev. Lett. 71, 1355 (1993).
- [54] S. F. Huelga, C. Macchiavello, T. Pellizzari, A. K. Ekert, M. B. Plenio, and J. I. Cirac, Phys. Rev. Lett. 79, 3865 (1997).
- [55] Q. Guan, G. W. Biedermann, A. Schwettmann, and R. J. Lewis-Swan, arXiv:2108.09272 (2021).
- [56] G. M. Tino, Quantum Sci. Technol. 6, 024014 (2021).
- [57] T. Bothwell, C. J. Kennedy, A. Aeppli, D. Kedar, J. M. Robinson, E. Oelker, A. Staron, and J. Ye, arXiv preprint arXiv:2109.12238 (2021).
- [58] C.-W. Chou, D. B. Hume, T. Rosenband, and D. J. Wineland, Science 329, 1630 (2010).
- [59] J. Grotti, S. Koller, S. Vogt, S. Häfner, U. Sterr, C. Lisdat, H. Denker, C. Voigt, L. Timmen, A. Rolland, et al., Nat. Phys. 14, 437 (2018).
- [60] M. Takamoto, I. Ushijima, N. Ohmae, T. Yahagi, K. Kokado, H. Shinkai, and H. Katori, Nat. Photonics 14, 411 (2020).
- [61] M. e. Tse, H. Yu, N. Kijbunchoo, A. Fernandez-Galiana, P. Dupej, L. Barsotti, C. D. Blair, D. D. Brown, S. E. Dwyer, A. Effler, et al., Phys. Rev. Lett. 123, 231107 (2019).
- [62] F. Acernese, M. Agathos, L. Aiello, A. Allocca, A. Amato, S. Ansoldi, S. Antier, M. Arène, N. Arnaud, S. Ascenzi, et al., Phys. Rev. Lett. 123, 231108 (2019).
- [63] C. J. Kennedy, E. Oelker, J. M. Robinson, T. Bothwell, D. Kedar, W. R. Milner, G. E. Marti, A. Derevianko, and J. Ye, Phys. Rev. Lett. 125, 201302 (2020).
- [64] J. Hu, W. Chen, Z. Vendeiro, A. Urvoy, B. Braverman, and V. Vuletić, Phys. Rev. A 96, 050301(R) (2017).
- [65] R. J. Lewis-Swan, M. A. Norcia, J. R. K. Cline, J. K. Thompson, and A. M. Rey, Phys. Rev. Lett. 121, 070403 (2018).
- [66] A. Chu, P. He, J. K. Thompson, and A. M. Rey, Phys. Rev. Lett. 127, 210401 (2021).

Supplementary Material: Bosonic pair production and squeezing for optical phase measurements in long-lived dipoles coupled to a cavity

Bhuvanesh Sundar,^{1, 2} Diego Barberena,^{1, 2} Asier Piñeiro Orioli,^{1, 2} Anjun Chu,^{1, 2} James K. Thompson,² Ana Maria Rey,^{1, 2} and Robert J. Lewis-Swan^{3, 4}

¹ Center for Theory of Quantum Matter, University of Colorado, Boulder, CO 80309, USA

² JILA, NIST, Department of Physics, University of Colorado, Boulder, CO 80309, USA

³ Homer L. Dodge Department of Physics and Astronomy,

The University of Oklahoma, Norman, OK 73019, USA

⁴ Center for Quantum Research and Technology, The University of Oklahoma, Norman, OK 73019, USA

PROPOSED EXPERIMENTAL IMPLEMENTATION

In the main text we introduced a proposal to realize an analog of bosonic four-wave mixing by coupling multilvel atoms to a far-detuned optical cavity mode. Here, we present a detailed discussion of the full atom-light Hamiltonian describing this system and show that it can be reduced to an effective spin model, which is presented as Eq. (1) in the main text.

Atom-light model

We consider multilevel atoms with a ground manifold and an excited manifold separated by an energy $\hbar\omega_a$, and 2F+1 Zeeman levels in each manifold. We denote the excited states as $|e,m\rangle$ and the ground states as $|g,m\rangle$ where the index $m\in [-F,F]$ specifies the Zeeman level. The cavity supports a pair of photon modes with degenerate angular frequency ω_c but different polarization. Without loss of generality, we take one of the cavity modes to be linearly polarized along the atomic quantization axis, which we call Π -polarization, and the other cavity mode to be linearly polarized perpendicular to the quantization axis, which we call Σ -polarization. The atoms couple to these two cavity modes with single-photon Rabi frequency $2g_0$.

The dynamics of the atom-light system is modeled by the Lindblad master equation,

$$\hbar \frac{d\rho}{dt} = -i[\hat{H}_{\text{tot}}, \rho] + \mathcal{L}_c[\rho] + \mathcal{L}_s[\rho]. \tag{S.1}$$

Here, $\hat{H}_{\text{tot}} = \hat{H}_A + \hat{H}_L + \hat{H}_{AL}$ is a Hamiltonian including contributions from the atoms, cavity modes, and atomlight coupling:

$$\hat{H}_{A} = \hbar \omega_{a} \hat{n}_{e} + \hbar (\delta_{g} \hat{F}_{g}^{z} + \delta_{e} \hat{F}_{e}^{z}),$$

$$\hat{H}_{L} = \hbar \omega_{c} \sum_{\alpha = \Pi, \Sigma} \hat{c}_{\alpha}^{\dagger} \hat{c}_{\alpha},$$

$$\hat{H}_{AL} = \hbar g_{0} \left(\hat{c}_{\Pi} \hat{\Pi}^{+} + \hat{c}_{\Sigma} \hat{\Sigma}^{+} + \text{h.c.} \right). \tag{S.2}$$

In the above equations, \hat{n}_e is the occupation in the excited manifold, $\hat{F}^z_{g(e)}$ =

 $\sum_{i=1}^{N}\sum_{m=-F}^{F}m\left|g(e),m\right\rangle_{i}\left\langle g(e),m\right| \text{ is the azimuthal spin operator for the ground (excited) manifold, and }\hat{c}_{\alpha} \text{ annihilates a photon in the cavity mode with polarization }\alpha. \text{ The terms }\hbar\delta_{g}\hat{F}_{g}^{z} \text{ and }\hbar\delta_{e}\hat{F}_{e}^{z} \text{ arise from Zeeman shifts due to an applied magnetic field.}$ The operators $\hat{\Sigma}^{+}(\hat{\Sigma}^{-})$ and $\hat{\Pi}^{+}(\hat{\Pi}^{-})$ are collective atomic operators that excite (de-excite) atoms by absorbing a Σ -polarized and Π -polarized cavity photon, respectively, given by $\hat{\Pi}^{+} = \sum_{i,m} C_{m}^{0} |e,m\rangle_{i} \left\langle g,m|$ and $\hat{\Sigma}^{+} = i\sum_{i,m,q=\pm 1} C_{m}^{q} |e,m+q\rangle_{i} \left\langle g,m|/\sqrt{2}, \text{ where } C_{m}^{q} = \left\langle F,m;1,q|F,m+q\right\rangle \text{ is the Clebsch-Gordan coefficient associated with exciting from }|g,m\rangle \text{ to }|e,m+q\rangle.$

It is convenient to move to a rotating frame that rotates at the atomic frequency ω_a . In this frame, the atomic angular frequency and cavity frequency are shifted by ω_a , yielding the Hamiltonian

$$\hat{H}_{\text{tot}} = \hbar (\delta_g \hat{F}_g^z + \delta_e \hat{F}_e^z) + \hbar \Delta \sum_{\alpha = \Pi, \Sigma} \hat{c}_{\alpha}^{\dagger} \hat{c}_{\alpha}$$
$$+ \hbar g_0 \left(\hat{c}_{\Pi} \hat{\Pi}^+ + \hat{c}_{\Sigma} \hat{\Sigma}^+ + \text{h.c.} \right), \qquad (S.3)$$

and we define the detuning of the cavity from the atomic transition, $\Delta = \omega_c - \omega_a$.

There are two Lindblad terms in the master equation (S.1), $\mathcal{L}_c[\rho]$ and $\mathcal{L}_s[\rho]$ that describe decoherence of the photon and atomic degrees of freedom. The former term captures leakage of photons out of the cavity at rate κ , and is given by

$$\mathcal{L}_{c}[\rho] = \hbar\kappa \sum_{\alpha = \Pi, \Sigma} \left(\hat{c}_{\alpha} \rho \hat{c}_{\alpha}^{\dagger} - \frac{1}{2} \hat{c}_{\alpha}^{\dagger} \hat{c}_{\alpha} \rho - \frac{1}{2} \rho \hat{c}_{\alpha}^{\dagger} \hat{c}_{\alpha} \right). \quad (S.4)$$

The second Lindblad term, $\mathcal{L}_s[\rho]$, models spontaneous decay of atoms from the excited manifold at rate γ ,

$$\mathcal{L}_{s}[\rho] = \sum_{i=1}^{N} \sum_{l=\pi,\sigma_{\pm}} \left(\hat{L}_{l,i}^{-} \rho \hat{L}_{l,i}^{+} - \frac{1}{2} \hat{L}_{l,i}^{+} \hat{L}_{l,i}^{-} \rho - \frac{1}{2} \rho \hat{L}_{l,i}^{+} \hat{L}_{l,i}^{-} \right). \tag{S.5}$$

This expression is further decomposed into three kinds of Lindblad jump operators: $\hat{L}_{\pi,i}^{-} = \sqrt{\hbar\gamma} \sum_{m} C_{m}^{0} \left| g, m \right\rangle_{i} \left\langle e, m \right| \text{ for spontaneous decay that preserves magnetization, and}$

 $\hat{L}_{\sigma_{\pm},i}^{-} = \sqrt{\hbar\gamma} \sum_{m} C_{m}^{\pm 1} |g,m\rangle_{i} \langle e,m\pm 1|$ for spontaneous decay that leads to a change in magnetization by ± 1 .

Effective spin model

When the cavity is detuned sufficiently far from the atomic transition, $|\Delta| \gg g_0 \sqrt{N}$, we can adiabatically eliminate the cavity photons and obtain an effective master equation for the atoms, $\hbar \frac{d\rho}{dt} = -i[\hat{H}, \rho] + \mathcal{L}_c[\rho] + \mathcal{L}_s[\rho]$ [1]. The effective Hamiltonian is

$$\hat{H} = \hbar \chi_0 \left(\hat{\Sigma}^+ \hat{\Sigma}^- + \hat{\Pi}^+ \hat{\Pi}^- \right) + \hbar (\delta_g \hat{F}_g^z + \delta_e \hat{F}_e^z), \quad (S.6)$$

where $\chi_0 \simeq -g_0^2/\Delta$ and the Lindblad terms are

$$\mathcal{L}_{c}[\rho] = \hbar \Gamma_{0} \left(\hat{\Pi}^{+} \rho \hat{\Pi}^{-} - \frac{1}{2} \hat{\Pi}^{+} \hat{\Pi}^{-} \rho - \frac{1}{2} \rho \hat{\Pi}^{+} \hat{\Pi}^{-} \right)$$

$$+ \hbar \Gamma_{0} \left(\hat{\Sigma}^{+} \rho \hat{\Sigma}^{-} - \frac{1}{2} \hat{\Sigma}^{+} \hat{\Sigma}^{-} \rho - \frac{1}{2} \rho \hat{\Sigma}^{+} \hat{\Sigma}^{-} \right),$$

$$\mathcal{L}_{s}[\rho] = \sum_{i=1}^{N} \sum_{l=\pi,\sigma_{\pm}} \left(\hat{L}_{l,i}^{-} \rho \hat{L}_{l,i}^{+} - \frac{1}{2} \hat{L}_{l,i}^{+} \hat{L}_{l,i}^{-} \rho - \frac{1}{2} \rho \hat{L}_{l,i}^{+} \hat{L}_{l,i}^{-} \right),$$
(S.7)

where $\Gamma_0 \approx g_0^2 \kappa/\Delta^2$. The terms in \hat{H} proportional to χ_0 are cavity photon-mediated exchange of atomic excitations, and the terms in $\mathcal{L}_c[\rho]$ capture collective decay of atoms from the excited manifold, also called superradiant decay.

As discussed in the main text, we consider initial conditions where half of the atoms are in $|q, m = -F\rangle$ and half in $|e, m = F\rangle$. Thus of all the exchange processes mediated by the cavity photons and written in Eq. (S.6), the dominant exchange occurs in the m = -F and m = Fsublevels, mediated by Π -polarized photons. The reason for this is that the Clebsch-Gordan coefficients are largest for these processes, $C_{+F}^0 = \pm \sqrt{F/(F+1)}$. The exchange process with the next highest amplitude, that exchanges atoms from $|g, -F\rangle |e, F\rangle$ to $|e, -F + 1\rangle |g, F - 1\rangle$ mediated by the exchange of Σ -polarized photon, has a smaller amplitude due to a smaller Clebsch-Gordan coefficient, $(C_F^{-1})^2 = 1/(F+1)$. Therefore, the populations in $|e, -F + 1\rangle$ and $|g, F - 1\rangle$ grow at an exponentially slower rate than in $|e, -F\rangle$ and $|q, F\rangle$. The amplitude of the process mediated by the Π -polarized photons, which exchanges atoms from $|g, -F\rangle |e, F\rangle$ to $|e, -F\rangle |g, F\rangle$, is proportional to $N\chi_0(C_F^0)^2$. At early times, the amplitudes of all the other exchange processes are at most $O(\sqrt{N}\chi_0)$.

Thus, keeping only the dominant exchange terms, from Eq. (S.6) we obtain the effective spin model [Eq. (1)] of the main text. The spin raising and lowering operators in Eq. (1) in the main text are the raising and lowering operators in Π^{\pm} projected into the

A and B manifolds, i.e. $\hat{S}_A^+ = \sum_i |e, -F\rangle_i \langle g, -F|, \hat{S}_B^+ = -\sum_i |e, F\rangle_i \langle g, F|,$ and the inversion operators are $\hat{S}_A^z = \sum_i (|e, -F\rangle_i \langle e, -F| - |g, -F\rangle) |g, -F\rangle)/2$ and $\hat{S}_B^z = \sum_i (|e, F\rangle_i \langle e, F| - |g, F\rangle)/2$. The Clebsch-Gordan coefficients that appeared in $\hat{\Pi}^\pm$ now do not appear in the spin operators $\hat{S}_{A,B}^\pm$, but are instead included the definition of the parameters in Eq. (1) as $\chi \approx -g_F^2/\Delta$, where $g_F = g_0 \sqrt{F/(F+1)}$, and $\delta = F(\delta_e - \delta_g)$.

To justify our argument that the effective spin model [Eq.(1)] in the main text] is the full spin Hamiltonian [Eq.(S.6)] projected into the $m=\pm F$ manifolds, we demonstrate that a numerical simulation of the dynamics of the full spin model [Eq.(S.6)] with all 2F+2 spin levels produces results consistent with an analytical prediction of the dynamics for the reduced effective spin model. In the next section, we describe how to analytically model the dynamics with an equivalent bosonic description of Eq.(1) and a subsequent approximation. In the section following that, we describe the numerical method that we use to simulate the full spin model [Eq.(1)].

DYNAMICS IN EQUIVALENT BOSONIC DESCRIPTION

In the main text, we reported analytic expressions for the internal state occupations $n_1(t)$ and $n_2(t)$ based on the reduction of the multilevel system discussed in Sec. [and Eq. (1) of the main text] to an ideal bosonic two-mode squeezing process. Here, we derive these analytic expressions within UPA. The expressions in the main text are for $\delta = N\chi/2$.

We start from the equivalent representation of Eq. (1) in the main text in terms of Schwinger bosons,

$$\begin{split} H = & \hbar \chi (\hat{a}_{e,A}^{\dagger} \hat{a}_{g,A} + \hat{a}_{e,B}^{\dagger} \hat{a}_{g,B}) (\hat{a}_{g,A}^{\dagger} \hat{a}_{e,A} + \hat{a}_{g,B}^{\dagger} \hat{a}_{e,B}) \\ &+ \frac{\hbar \delta}{2} (\hat{a}_{e,B}^{\dagger} \hat{a}_{e,B} - \hat{a}_{g,B}^{\dagger} \hat{a}_{g,B} - \hat{a}_{e,A}^{\dagger} \hat{a}_{e,A} + \hat{a}_{g,A}^{\dagger} \hat{a}_{g,A}). \end{split} \tag{S.8}$$

Under the UPA, we replace $\hat{a}_{g,A}^{\dagger}\hat{a}_{g,A}=\frac{N}{2}-\hat{a}_{e,A}^{\dagger}\hat{a}_{e,A}$, $\hat{a}_{e,B}^{\dagger}\hat{a}_{e,B}=\frac{N}{2}-\hat{a}_{g,B}^{\dagger}\hat{a}_{g,B}$, and $\hat{a}_{g,A}^{\dagger}\approx\hat{a}_{e,B}^{\dagger}\approx\sqrt{\frac{N}{2}}$. Then, the Hamiltonian (S.8) reduces to

$$\begin{split} H \approx & \frac{N\hbar\chi}{2} (\hat{a}_{e,A}^{\dagger} + \hat{a}_{g,B}) (\hat{a}_{e,A} + \hat{a}_{g,B}^{\dagger}) \\ & - N\hbar\delta (\hat{a}_{e,A}^{\dagger} \hat{a}_{e,A} + \hat{a}_{g,B}^{\dagger} \hat{a}_{g,B}). \end{split} \tag{S.9}$$

Since the Hamiltonian (S.9) is quadratic in Schwinger boson operators, the Heisenberg time evolution of these operators can be analytically solved by integrating the matrix equation

$$i\partial_t \begin{pmatrix} \hat{a}_{e,A} \\ \hat{a}_{q,B}^{\dagger} \end{pmatrix} = \begin{pmatrix} \frac{N\chi}{2} - \delta & \frac{N\chi}{2} \\ -\frac{N\chi}{2} & -\frac{N\chi}{2} + \delta \end{pmatrix} \begin{pmatrix} \hat{a}_{e,A} \\ \hat{a}_{q,B}^{\dagger} \end{pmatrix}.$$
(S.10)

The occupations are then obtained as,

$$n_{e,A}(t)=n_{g,B}(t)=\frac{(N\chi)^2}{4\delta(N\chi-\delta)}\sinh^2\Big(t\sqrt{}$$

When $\delta = N\chi/2$ the Zeeman shift cance field energy shift [corresponding to the el tion terms in (S.8)], making the pair pro nant. Then, the occupations grow the fastes $n_{g,B}(t) = \sinh^2 \frac{N\chi t}{2}$.

THE TRUNCATED WIGNER APPRO

In the main text, we used UPA to pred lation growth and sensitivity of our protoc assumed that only four out of 4F+2 levels for the dynamics, with relevant interactions Π -polarized photons only, and gave analytic the ensuing dynamics. In Fig. 1(d) in the 1 benchmarked the UPA predictions for the sensults obtained from the truncated Wignetion (TWA). In this section, we describe the benchmark the dynamics of pair creation.

The TWA is a semiclassical method who expectation values of observables by averagensemble of trajectories, and each trajector by integrating classical equations of motion ues of operators sampled from a probability which properly accounts for quantum fluct

Specifically, we integrate classical equation for collective multilevel spin opera $\sum_i |\alpha\rangle_i \langle\beta|_i$, where α and β can be a groun or an excited state (e,m). There are (4F+ operators. Their initial values are sampled variate Gaussian distribution with mean a matrix given by the mean and covariance state,

$$\mu_{\alpha\beta} = \langle \hat{S}_{\alpha\beta} \rangle ,$$

$$\sigma_{\alpha\beta,\gamma\delta} = \sqrt{\frac{1}{2} \langle \hat{S}_{\alpha\beta} \hat{S}_{\gamma\delta} + \hat{S}_{\gamma\delta} \hat{S}_{\alpha\beta} \rangle - \langle \hat{S}_{\alpha\beta} \rangle} ,$$

After creating an ensemble of initial values $\{S_{\alpha\beta}(t=0)\}$, each initial value is then propagated according to their equations of motion (see below).

To obtain the equations of motion, it is convenient to first write the Hamiltonian in short-hand notation as

$$\hat{H} = \sum_{\alpha\beta} h_{\alpha\beta} \hat{S}_{\alpha\beta} + \sum_{\alpha\beta\gamma\delta} h_{\alpha\beta\gamma\delta} \hat{S}_{\alpha\beta} \hat{S}_{\gamma\delta}.$$
 (S.13)

Here, $h_{\alpha\beta}$ are single-particle terms due to the magnetic field, and $h_{\alpha\beta\gamma\delta}$ are interaction terms. For our system, $h_{\alpha\beta}$ is a diagonal matrix. The Heisenberg equations for

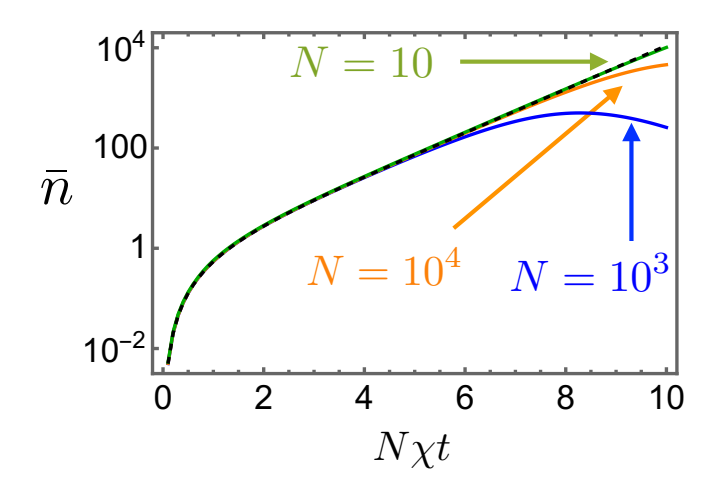


FIG. S.1. Growth of number of entangled particles \bar{n} for $\delta = N\chi/2$. Solid curves obtained from TWA agree well with the UPA prediction (dashed curve) until $\bar{n} \sim 0.1N$

the multilevel operators can be written schematically as

$$i\partial_t \hat{S}_{\alpha\beta}(t) = [\hat{S}_{\alpha\beta}, \hat{H}] = \sum_{\mu\nu} \Lambda^{\mu\nu}_{\alpha\beta} \hat{S}_{\mu\nu} + \sum_{\mu\nu\lambda\sigma} \Lambda^{\mu\nu\lambda\sigma}_{\alpha\beta} \hat{S}_{\mu\nu} \hat{S}_{\lambda\sigma}$$
(S.14)

where $\Lambda^{\mu\nu}_{\alpha\beta}$ depends on the single-particle terms, and $\Lambda^{\mu\nu\lambda\sigma}_{\alpha\beta}$ depends on the interactions. To obtain the classical equations of motion, we replace quantum operators with their classical counterparts. Monomial operators are replaced as $\hat{S}_{\alpha\beta} \to S_{\alpha\beta}$, and quadratic operators are replaced by a symmetric decoupling scheme, $\frac{1}{2}\{\hat{S}_{\alpha\beta},\hat{S}_{\gamma\delta}\}\to S_{\alpha\beta}S_{\gamma\delta}$. Subsequently, we integrate these equations using a standard differential equation solver.

Observables are computed by averaging over trajectories. For instance, occupations are obtained from $n_{\alpha}(t) = \overline{S_{\alpha\alpha}(t)}$, where $\overline{\cdots}$ denotes ensemble average.

The numerical results in Fig. 1(d), computed by simulating for the full spin model [Eq. (S.6)] under the TWA, agree excellently with the UPA prediction for the squeezing. In Fig. S.1, we again find excellent agreement between the UPA prediction and TWA calculation of the number of entangled pairs produced, \bar{n} . These results support our arguments that the effective spin model is given by Eq.(1) in the main text, and that the dynamics can be reasonably treated under UPA.

DESCRIPTION OF THE SQUEEZING IN JOINT BLOCH SPHERES

An important and well known feature of the bosonic model of pair production [Eqs. (S.8) and (S.9)] is that it generates squeezing in joint quadratures of the two bosonic modes. In this section, we show that this implies that, within UPA, our spin model is also capable of generating spin squeezing of combined spin quadratures of

the A and B ensembles.

To be concrete, we consider only the case with $\delta = N\chi/2$ so that our effective spin Hamiltonian \hat{H} [see Eq. (1) of the main text)] reduces to

$$\hat{H} = \hbar \chi (\hat{S}_A^+ \hat{S}_B^- + \hat{S}_B^+ \hat{S}_A^-). \tag{S.15}$$

We begin by rewriting this Hamiltonian in a more convenient form,

$$\hat{H} = 2\hbar \chi (\hat{S}_A^x \hat{S}_B^x + \hat{S}_A^y \hat{S}_B^y), \tag{S.16}$$

which can be alternatively factorized as,

$$\hat{H} = \hbar \chi \left(\hat{S}_B^y + \hat{S}_A^x \right) \left(\hat{S}_B^x + \hat{S}_A^y \right) - \hbar \chi \left(\hat{S}_B^y - \hat{S}_A^x \right) \left(\hat{S}_B^x - \hat{S}_A^y \right). \quad (S.17)$$

To proceed, let us denote the terms appearing in Eq. (S.17) as $S_{1,+} = \hat{S}_B^x + \hat{S}_A^y$, $S_{2,+} = \hat{S}_B^y + \hat{S}_A^x$, $S_{1,-} = \hat{S}_B^x - \hat{S}_A^y$, and $S_{2,-} = \hat{S}_B^y - \hat{S}_A^x$. As we will see below, this new notation will enable us to gain physical intuition by visualizing the physics as occurring on two independent Bloch spheres. We define a third axis, $S_{3,-} = \hat{S}_B^z - \hat{S}_A^z$, which enables us to identify that $(S_{1,+}, S_{2,+}, S_{3,-})$ and $(S_{1,-}, S_{2,-}, S_{3,-})$ each independently satisfy the canonical commutation relations of SU(2) spins. Therefore, we can construct two Bloch spheres with a shared axis, with the first sphere's axes as $(S_{1,+}, S_{2,+}, S_{3,-})$ and the second sphere's axes as $(S_{1,-}, S_{2,-}, S_{3,-})$. The first line of Eq. (S.17) acts only on the first Bloch sphere, and the second line acts only on the second Bloch sphere.

The generation of squeezing by \hat{H} can be understood by mapping the axes of the Bloch spheres to bosonic quadratures, which translates \hat{H} to a form that is familiar in quantum optics. At the mean-field level (equivalently, in the UPA), $\mathcal{S}_{3,-}$ is a constant of motion with value N/2. Therefore, in this approximation, $\mathcal{S}_{1,+}$ and $\mathcal{S}_{2,+}$ can be mapped to bosonic quadratures \hat{X}_+ and \hat{Y}_+ as $\mathcal{S}_{1,+} \approx \sqrt{\frac{N}{2}}\hat{X}_+$ and $\mathcal{S}_{2,+} \approx \sqrt{\frac{N}{2}}\hat{Y}_+$, which satisfy the canonical commutation relation $[\hat{X}_+,\hat{Y}_+]=i$. We similarly define $\mathcal{S}_{1,-} \approx \sqrt{\frac{N}{2}}\hat{X}_-$ and $\mathcal{S}_{2,-} \approx \sqrt{\frac{N}{2}}\hat{Y}_-$, where $[\hat{X}_-,\hat{Y}_-]=i$. The Hamiltonian, written in terms of these bosonic quadratures, is

$$\hat{H} = \frac{N\hbar\chi}{2}\hat{Y}_{+}\hat{X}_{+} - \frac{N\hbar\chi}{2}\hat{Y}_{-}\hat{X}_{-}.$$
 (S.18)

It is well-known that this Hamiltonian generates squeezing along \hat{Y}_+ and \hat{X}_- for $\chi > 0$ (and conversely, along \hat{X}_+ and \hat{Y}_- for $\chi < 0$) [3]. Equivalently, we must have that our Hamiltonian generates squeezing in two spin quadratures along $\mathcal{S}_{2,+}$ and $\mathcal{S}_{1,-}$ respectively for $\chi > 0$. This is the two-mode squeezing that we report in the main text. The squeezing manifests itself as reduced quantum noise,

$$var(S_{1,-}) = var(S_{2,+}) = \frac{N}{4}e^{-\chi Nt},$$
 (S.19)

and the anti-squeezing as increased quantum noise,

$$var(S_{2,-}) = var(S_{1,+}) = \frac{N}{4}e^{\chi Nt}.$$
 (S.20)

The squeezing/anti-squeezing is well-defined relative to the isotropic projection noise associated with a typical coherent spin state on each of the independent collective Bloch spheres, characterized by $\operatorname{var}(\mathcal{S}_{1,\pm}) = \operatorname{var}(\mathcal{S}_{2,\pm}) = N/4$ for our initial state polarized along $\mathcal{S}_{3,-}$.

Lastly, we briefly discuss the illustrations of the quantum noise in Fig. 1(c) of the main text. The dynamics, and in particular the squeezing, produced by the bosonic Hamiltonian $\hat{H}=\frac{N\hbar\chi}{2}\hat{Y}_{+}\hat{X}_{+}-\frac{N\hbar\chi}{2}\hat{Y}_{-}\hat{X}_{-}$ can be understood via the Wigner function computed in terms of the bosonic quadratures. It is well known that the Wigner function of two-mode squeezed vacuum factorizes into a pair of single-mode squeezed states with respect to the independent phase-spaces defined by (X_{\perp}, Y_{\perp}) and (X_{-},Y_{-}) . The axes describing these two phase spaces commute with each other. Strictly, when the UPA is satisfied we can transplant each of these bosonic phasespaces (up to prefactors) to lie on the surface of the independent Bloch spheres defined by $(S_{1,+}, S_{2,+}, S_{3,-})$ and $(S_{1,-}, S_{2,-}, S_{3,-})$ by ignoring the curvature effects [i.e., the spin Wigner functions are effectively limited to the 2D planes $(S_{1,+}, S_{2,+})$ and $(S_{1,-}, S_{2,-})$, where the spin Wigner functions on each Bloch sphere lie on axes that commute with their counterparts on the other Bloch sphere, assuming the pump populations are equal. We adopt this correspondence for Fig. 1(c) to schematically illustrate the spin-squeezing in this spirit. For illustrative purposes, we enlarge the area covered by the spin Wigner functions, while strictly within the UPA, they are restricted to an infinitesimal surface perpendicular to $S_{3,-}$.

EVOLUTION OF THE JOINT BLOCH SPHERES DURING THE RAMSEY SEQUENCE

In the main text, we visualized the Ramsey sequence as rotations of the spin distribution on the lower Bloch sphere of Fig. 1(c). Here, we describe the evolution of the spin distribution on the upper Bloch sphere during the Ramsey sequence.

We first consider the Ramsey sequence that measures the differential phase [illustrated in Fig. 2(a) in the main text]. After the first pulse, realized by $\exp\left(-i\frac{\pi}{2}\hat{\mathcal{S}}_{2,+}\right)$, the axes on the upper Bloch sphere are rotated from $(\mathcal{S}_{1,-},\mathcal{S}_{2,-},\mathcal{S}_{3,-})$ to $(-\mathcal{S}_{3,+},\mathcal{S}_{2,-},\mathcal{S}_{1,+})$. This is illustrated in Fig. S.2(a). The Bloch vector points along $\mathcal{S}_{1,+}$, which is now a shared axis with the other Bloch sphere [see Fig. 2(a)]. At this step, the system is a null state of $\mathcal{S}_{1,-}$, assuming the initial pump populations were equal.

The next step in the Ramsey sequence is a small rotation ϕ of the Bloch vector. In the main text, we consid-

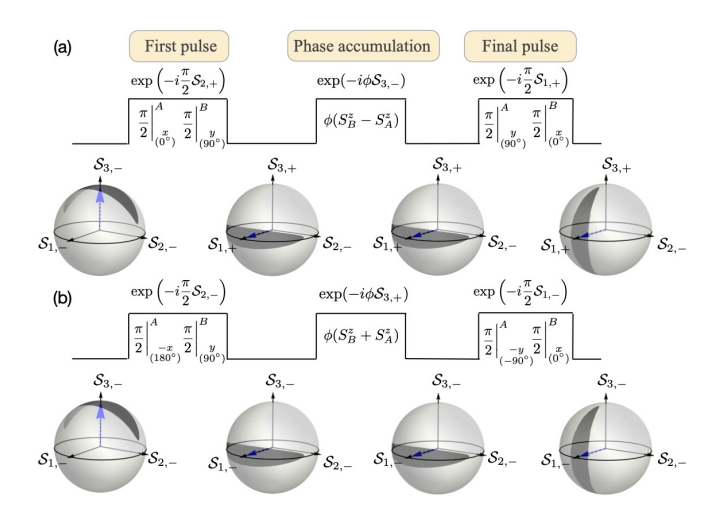


FIG. S.2. Evolution of the spin distributions in the upper Bloch sphere in Fig. 1(c) in the main text, during the Ramsey sequence for measuring (a) the differential phase, (b) the sum phase. Information about the imprinted phase is not captured in the spheres shown here. Dashed blue arrows show the Bloch vector.

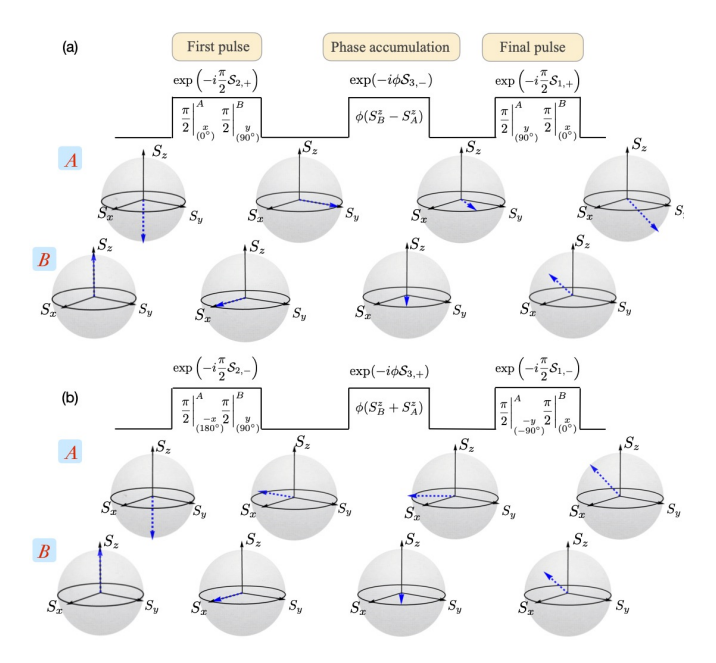


FIG. S.3. Rotation of the Bloch vectors in the A and B ensembles during the Ramsey sequence for measuring (a) the differential phase, (b) the sum phase.

ered a rotation generated by $\exp(-i\phi S_{3,-})$. This operation does not rotate the spin distribution in Fig. S.2(a). This is because in UPA, the spin distribution lies entirely in the plane $(S_{3,+}, S_{2,-})$, and these two axes commute with $\exp(-i\phi S_{3,-})$, if the initial pump populations were equal. The rotation generated by $\exp(-i\phi S_{3,-})$ only rotates the spin distribution in the Bloch sphere shown in the main text.

The final step in the Ramsey sequence is a rotation

implemented by $\exp\left(-i\frac{\pi}{2}\mathcal{S}_{1,+}\right)$, which rotates the spin distribution by 90°. Figure S.2(a) shows that the total atomic inversion encodes no information about ϕ , i.e. $\langle \hat{S}_A^z + \hat{S}_B^z \rangle = 0$. Conversely, Fig. 2(a) (main text) showed that the difference in atomic inversions, $\langle \hat{S}_B^z - \hat{S}_A^z \rangle$, encoded information about ϕ .

Fig. S.2(b) shows how the upper Bloch sphere in Fig. 1(c) evolves during the Ramsey protocol that measures the sum phase. No information about the imprinted sum phase is captured by the sphere in Fig. S.2(b).

For ease of understanding, we also show in Fig. S.3 how the Bloch vectors in the A and B ensembles separately evolve during the two Ramsey protocols.

ACHIEVABLE SENSITIVITY INCORPORATING INTRINSIC DECOHERENCE

In this section, we sketch how we compute the sensitivity of our protocol in the presence of decoherence. We begin by writing the master equation for \hat{S}_A^\pm and \hat{S}_B^\pm , analogous to Eq. (S.10), but now including decoherence as well. The two sources of decoherence that we consider are collective decay and independent spontaneous decay of atoms from the excited states. These two decoherences have two main effects: they reduce coherences, and cause depletion of the excited modes. This will require us to go beyond the UPA, since the excited mode in the B ensemble is a pump mode, and it gets depleted by decay to the ground state. As a further effect of pump depletion, the Zeeman shift does not cancel the mean-field energy shift. We will account for this as well.

The master equation is

$$\begin{split} \partial_t \left(\begin{array}{c} \langle \hat{S}_A^- \rangle \\ \langle \hat{S}_B^- \rangle \end{array} \right) &\approx \left(\begin{array}{cc} -\frac{\gamma}{2} + i\delta & 0 \\ 0 & -\frac{\gamma}{2} - i\delta \end{array} \right) \left(\begin{array}{c} \langle \hat{S}_A^- \rangle \\ \langle \hat{S}_B^- \rangle \end{array} \right) \\ &+ (\Gamma + 2i\chi) \left(\begin{array}{cc} \langle \hat{S}_A^z \rangle & \langle \hat{S}_A^z \rangle \\ \langle \hat{S}_B^z \rangle & \langle \hat{S}_B^z \rangle \end{array} \right) \left(\begin{array}{c} \langle \hat{S}_A^- \rangle \\ \langle \hat{S}_B^- \rangle \end{array} \right), \end{split} \tag{S.21}$$

where we have approximated that $\langle \hat{S}_A^z \hat{S}_B^- \rangle \approx \langle \hat{S}_A^z \rangle \langle \hat{S}_B^- \rangle$ and similarly for $A \leftrightarrow B$. Since spontaneous decay causes the excited populations to decrease with time, we have to modify the undepleted pump approximation, $\langle \hat{S}_B^z \rangle = \frac{N}{4}$, to $\langle \hat{S}_B^z \rangle = \frac{N}{4}(2e^{-\gamma t}-1)$. We set $\langle \hat{S}_A^z \rangle = -N/4$, since there is no initial excited population in the A ensemble. We choose $\delta = \frac{N_X}{2}$ as we did in the main text.

Equation (S.21) is a time-dependent coupled differential equation which is non-trivial to solve. Instead, we solve Eq. (S.21) to first order in Γ and γ . Separating the matrix on the right hand side as $M = M_0 + M_1(t)$, where M_0 is the contribution at $\Gamma = \gamma = 0$, and $M_1(t)$ is the

remaining contribution, the solution to Eq. (S.21) is

$$\begin{pmatrix}
\langle \hat{S}_{A}^{-}(t) \rangle \\
\langle \hat{S}_{B}^{-}(t) \rangle
\end{pmatrix} = \left(e^{M_{0}t} + \int_{0}^{t} d\tau \ e^{M_{0}(t-\tau)} M_{1}(\tau) e^{M_{0}\tau} \right) \\
\times \left(\langle \hat{S}_{A}^{-}(0) \rangle \\
\langle \hat{S}_{B}^{-}(0) \rangle \right).$$
(S.22)

Similar equations can be set up and solved for the second moments, $\langle \hat{S}_A^+ \hat{S}_B^- \rangle$, $\langle \hat{S}_A^+ \hat{S}_A^- \rangle$, and $\langle \hat{S}_B^+ \hat{S}_B^- \rangle$, which are necessary for calculating the squeezed quantum noise.

In the Ramsey protocol that measures the differential phase, the value of the signal measured is

$$\langle \hat{S}_B^z - \hat{S}_A^z \rangle_{\text{final}} = \langle \hat{S}_B^z(t) - \hat{S}_A^z(t) \rangle \sin \phi + \langle \hat{S}_B^y(t) + \hat{S}_A^x(t) \rangle \cos \phi, \qquad (S.23)$$

where t is the time before the first $\pi/2$ pulse in the Ramsey sequence. The first term in the above equation is $-\frac{N}{2}e^{-\gamma t}\sin\phi$, and the second term is zero. The fluctuation in the signal is

$$\begin{split} &\langle \Delta (\hat{S}_B^z - \hat{S}_A^z)^2 \rangle_{\text{final}} = \langle \Delta (\hat{S}_B^z(t) - \hat{S}_A^z(t))^2 \rangle \sin^2 \phi \\ &+ \langle \Delta (\hat{S}_B^y(t) + \hat{S}_A^x(t))^2 \rangle \cos^2 \phi \\ &+ \cos \phi \sin \phi \, \langle \Delta (\hat{S}_B^z(t) - \hat{S}_A^z(t)) \Delta (\hat{S}_B^y(t) + \hat{S}_A^x(t)) \rangle \\ &+ \cos \phi \sin \phi \, \langle \Delta (\hat{S}_B^y(t) + \hat{S}_A^x(t)) \Delta (\hat{S}_B^z(t) - \hat{S}_A^z(t)) \rangle \,. \end{split} \tag{S.24}$$

The best sensitivity is achieved at $\phi = 0$, therefore we set $\phi = 0$ hereafter. Solving for the second order moments in a similar fashion to Eq. (S.22), the fluctuation in the signal is

$$\begin{split} \langle \Delta (\hat{S}_B^z - \hat{S}_A^z)^2 \rangle_{\text{final}} &= \frac{N}{4} \left(e^{-N\chi t} + \frac{\Gamma}{2\chi} + \frac{\gamma}{N\chi} \right. \\ &+ e^{N\chi t} \left(\frac{\Gamma}{4\chi} + \frac{\gamma}{2N\chi} - \frac{\gamma t}{2} \right)^2 + e^{N\chi t} \left(\frac{\gamma}{2N\chi} - \frac{\gamma t}{2} \right)^2 \right). \end{split} \tag{S.25}$$

This yields the sensitivity as

$$(\Delta\phi)^2 = \frac{e^{-N\chi t}}{N} + \frac{\Gamma}{2N\chi} + \frac{\gamma}{N^2\chi} + \frac{e^{N\chi t}}{N} \left(\frac{\gamma}{2N\chi} - \frac{\gamma t}{2}\right)^2 + \frac{e^{N\chi t}}{N} \left(\frac{\Gamma}{4\chi} + \frac{\gamma}{2N\chi} - \frac{\gamma t}{2}\right)^2.$$
 (S.26)

An analysis for the Ramsey protocol that measures the sum phase yields the same expression for the sensitivity.

SCALING OF $(\Delta \phi_{\min})^2$ WITH N.

The best sensitivity is achieved at optimum values of Δ and t. These optimum values aim to find the right balance between the gain obtained by reaching a higher \bar{n}

versus the loss in squeezing due to decoherence. We find the optimum values of Δ and t by setting the derivatives of $\Delta \phi^2$ with respect to Δ and t as zero.

First, we find the optimum duration for our protocol. This is obtained by setting $d(\Delta\phi)^2/dt=0$, which yields the implicit equation

$$\gamma t = \frac{\Gamma}{4\chi} + \sqrt{2e^{-2N\chi t} + \left(\frac{\gamma}{N\chi}\right)^2 - \left(\frac{\Gamma}{4\chi}\right)^2}.$$
 (S.27)

We approximate this time as $\gamma t \approx \frac{\Gamma}{4\chi} + \sqrt{2}e^{-N\Gamma/4\gamma}$. At this optimum time, the sensitivity is given by

$$N(\Delta\phi)^{2} = \exp\left(-\frac{N\Gamma}{4\gamma} - \frac{\sqrt{2}N\chi}{\gamma}e^{-N\Gamma/4\gamma}\right) + \frac{\Gamma}{2\chi} + \frac{\gamma}{N\chi} + \exp\left(\frac{N\Gamma}{4\gamma} + \frac{\sqrt{2}N\chi}{\gamma}e^{-N\Gamma/4\gamma}\right) \times \left(\frac{\gamma^{2}}{N^{2}\chi^{2}} + e^{-N\Gamma/2\gamma} - \frac{\sqrt{2}\gamma}{N\chi}e^{-N\Gamma/4\gamma}\right).$$
(S.28)

The parameters Γ and χ depend on the cavity detuning Δ and the cavity loss rate κ as $\chi = \frac{g_F^2}{\Delta}$ and $\Gamma = \frac{g_F^2 \kappa}{\Delta^2}$. Rewriting the sensitivity in terms of Δ , κ , and the cavity cooperativity $C = \frac{4g_F^2}{\kappa \gamma}$, we optimize the sensitivity with respect to Δ . This gives us an optimum value of Δ ,

$$\Delta \approx \sqrt{\frac{NC}{2\ln(2NC)}}\kappa.$$
 (S.29)

The optimum sensitivity at this detuning is given by

$$N(\Delta\phi)^2 \approx \sqrt{\frac{2\ln(2NC)}{NC}}.$$
 (S.30)

EFFECT OF PUMP POPULATION FLUCTUATIONS ON THE SENSITIVITY

Here, we calculate the sensitivity for the case that the initial pump populations are unequal. We denote the populations in the pump states $|g,A\rangle$ and $|e,B\rangle$ as $N_{g,A}$ and $N_{g,B}$.

First we consider the symmetric choice $N_{g,A} = \frac{N + \delta N}{2}$, $N_{e,B} = \frac{N - \delta N}{2}$, and $\delta N \ll N$, which has nonzero difference $N_{g,A} - N_{e,B} = \delta N$ but no fluctuation in the sum. As before, we write the equivalent bosonic representation of Eq.(1) in the main text in terms of Schwinger bosons, and make the UPA. The Heisenberg equation of motion for $\hat{a}_{e,A}$ and $\hat{a}_{g,B}$ are given by

$$i\partial_t \left(\begin{array}{c} \hat{a}_{e,A} \\ \hat{a}_{g,B}^\dagger \end{array} \right) = \left(\begin{array}{cc} N_{g,A}\chi - \delta & \sqrt{N_{g,A}N_{e,B}}\chi \\ -\sqrt{N_{g,A}N_{e,B}}\chi & -N_{e,B}\chi + \delta \end{array} \right) \left(\begin{array}{c} \hat{a}_{e,A} \\ \hat{a}_{g,B}^\dagger \end{array} \right). \tag{S.31}$$

Solving this equation analytically, we find that the squeezing in $S_{2,+}$ and $S_{1,-}$ are modified to

$$var(S_{2,+}(t)) = var(S_{1,-}(t)) \simeq \frac{N}{4}e^{-N\chi t} + \frac{\delta N}{2}.$$
 (S.32)

The sensitivity of our Ramsey protocol at $\phi = 0$ is

$$(\Delta \phi)^2 = \frac{\operatorname{var}(\mathcal{S}_{1,-}(t))}{\langle \mathcal{S}_{3,-}(t) \rangle^2}.$$
 (S.33)

For the symmetric choice $N_{g,A}=\frac{N+\delta N}{2},\ N_{e,B}=\frac{N-\delta N}{2}$ and within UPA, we have $\langle \mathcal{S}_{3,-}(t)\rangle\simeq\frac{N}{2}$, and var $(\mathcal{S}_{1,-}(t))$ is in Eq. (S.32). These results lead to

$$(\Delta \phi)^2 \simeq \frac{e^{-N\chi t}}{N} + \frac{\delta N}{N}.$$
 (S.34)

An ensemble of experiments typically have fluctuations in populations $\delta N \sim O(\sqrt{N})$. The correction to the sensitivity for this magnitude of fluctuation scales with N in the same way as the corrections obtained from decoherence and from effects beyond UPA.

A similar calculation of the sensitivity with fluctuation in the sum population shows that the sensitivity only depends quadratically on the sum fluctuation.

PAIR PRODUCTION WITH SPIN-1 BECS

In the main text we contrast our effective bosonic model with alternative realization in quantum optics and spinor Bose-Einstein condensates. In the latter case, degenerate four-wave mixing is engineered through s-wave atomic collisions that change the internal Zeeman state of the atoms [4]. It is common to simplify the theoretical treatment of the atomic collisions by invoking a single mode approximation (SMA), wherein it is assumed that all atoms share the same spatial wavefunction, regardless of their internal Zeeman state. This is typically valid for small systems and short to intermediate timescales, although a range of factors contribute [5].

By freezing out the spatial degree of freedom via the SMA the internal state dynamics for a spin-1 BEC is then given by,

$$\hat{H}_{BEC} = \frac{U_s}{2N} \hat{\vec{S}} \cdot \hat{\vec{S}} + q(\hat{n}_1 + \hat{n}_{-1}).$$
 (S.35)

Here, the spin operators are $\hat{S}_x=(\hat{a}_1^{\dagger}\hat{a}_0+\hat{a}_0^{\dagger}\hat{a}_{-1}+\text{h.c.})/\sqrt{2}$, $\hat{S}_y=(\hat{a}_1^{\dagger}\hat{a}_0+\hat{a}_0^{\dagger}\hat{a}_{-1}-\text{h.c.})/\sqrt{2}i$, and $\hat{S}_z=\hat{a}_1^{\dagger}\hat{a}_1-\hat{a}_{-1}^{\dagger}\hat{a}_{-1}$, where \hat{a}_m^{\dagger} creates a boson in Zeeman sublevel $m=0,\pm 1$. The first term of Eq. (S.35) describes

spin-mixing due to s-wave atomic collisions characterized by interaction strength U_s , whereas the second term describes a quadratic Zeeman shift $q \propto B^2$ due to an applied magnetic field.

The Hamiltonian (S.35) can be rewritten in a more insightful form, $\hat{H}_{BEC} = \hat{H}_{inel} + \hat{H}_{el} + \hat{H}_{Z}$ with [6]

$$\hat{H}_{\text{inel}} = \frac{U_s}{N} \left(\hat{a}_0 \hat{a}_0 \hat{a}_1^{\dagger} \hat{a}_{-1}^{\dagger} + h.c. \right),$$

$$\hat{H}_{\text{el}} = \frac{U_s}{N} \hat{n}_0 \left(\hat{n}_1 + \hat{n}_{-1} \right) + \frac{U_s}{2N} \left(\hat{n}_1 - \hat{n}_{-1} \right)^2, \qquad (S.36)$$

$$\hat{H}_Z = q(\hat{n}_1 + \hat{n}_{-1}).$$

The first term, $\hat{H}_{\rm inel}$, describes spin-changing collisions wherein a pair of m=0 atoms collide and scatter into an $m=\pm 1$ pair. Conversely, the second term, $\hat{H}_{\rm el}$, describes elastic collisions which preserve the relative spin populations. Inspection of $\hat{H}_{\rm BEC}$ in this form shows that, up to the distinguishing feature that the spin-1 BEC involves only three bosonic modes, it is analogous to the four-wave mixing Hamiltonian for our system described in Eq. (S.8).

Many experiments probe the regime where a BEC is prepared with the vast majority of atoms in the m=0 state. For large systems the UPA then corresponds to replacing $\hat{a}_0 \approx \sqrt{N}$ where N is the number of atoms in the condensate. Equation (S.35) then reduces to

$$\hat{H}_{\text{BEC}} \approx (q + U_s)(\hat{a}_1^{\dagger} \hat{a}_1 + \hat{a}_{-1}^{\dagger} \hat{a}_{-1}) + U_s(\hat{a}_1^{\dagger} \hat{a}_{-1}^{\dagger} + \text{h.c.}).$$
(S.37)

where we have ignored a term $\propto \hat{a}_1^{\dagger} \hat{a}_1 - \hat{a}_{-1}^{\dagger} \hat{a}_{-1}$ as a conserved quantity. Within the UPA, the spin-1 Hamiltonian is thus analogous to $\hat{H}_{\rm TMS}$ in Eq. (3) in the main text, with $U_s = N\hbar\chi/2$, and $q = \hbar\delta$. The resonant condition for pair production is met when $q = -U_s$.

- J. A. Muniz, D. Barberena, R. J. Lewis-Swan, D. J. Young, J. R. K. Cline, A. M. Rey, and J. K. Thompson, Nature 580, 602 (2020).
- [2] A. Polkovnikov, Ann. Phys. **325**, 1790 (2010).
- [3] G. S. Agarwal, Quantum optics (Cambridge University Press, 2012).
- [4] C. K. Law, H. Pu, and N. P. Bigelow, Phys. Rev. Lett. 81, 5257 (1998).
- [5] J. Jie, Q. Guan, S. Zhong, A. Schwettmann, and D. Blume, Phys. Rev. A 102, 023324 (2020).
- [6] Q. Guan, G. W. Biedermann, A. Schwettmann, and R. J. Lewis-Swan, arXiv:2108.09272 (2021).